Advective transport in the percolation backbone in two dimensions

Jean-Raynald de Dreuzy,[1,2] Philippe Davy,[1] and Brian Berkowitz[2]
[1]*Géosciences Rennes, UMR 6118 CNRS, Université de Rennes 1, Campus de Beaulieu, 35042 Rennes Cedex, France*
[2]*Environmental Sciences, Weizmann Institute of Science, 76100 Rehovot, Israel*
(Received 11 June 2001; published 24 October 2001)

We show that, in the case of advective transport on the percolation backbone, the relevant structure below the correlation length is an ensemble of tortuous paths, rather than the classical links-nodes-blobs system. These paths are embedded in the few largest blobs that dominate the structure of the backbone. We find numerically that the mean particle displacement differs from the prediction given by classical finite-size scaling arguments. We also show that because of the complex velocity distribution between the paths, the mean first-passage time of the particles cannot be inferred directly from the mean particle displacement.

DOI: 10.1103/PhysRevE.64.056305 PACS number(s): 47.55.Mh, 64.60.Ak, 91.60.−x

Numerous environmental issues, such as the storage of nuclear wastes in underground repositories, require the understanding and modeling of chemical transport in geological formations. This problem has been addressed experimentally in different porous and fractured media [1,2] and theoretically by a broad range of frameworks [3,4]. The structure of the percolation cluster at criticality is a useful model for numerous porous and fractured media [5,6]. While diffusive processes on the percolating cluster have been treated by many studies [7], fewer studies have considered advective processes [8–11]. In the pure advective case, the mean velocity and the dispersivity on percolating clusters have been estimated in systems of increasing sizes using finite-size scaling arguments explicitly [8] or implicitly [9–11] to infer the temporal evolution of the particles within a given system.

We compute directly the mean particle velocity and the dispersivity of advected ''particles'' (representing chemical mass) within percolation systems, and find, below the correlation length, different predictions from the one given by finite-size scaling arguments. We show that both the classical finite-size scaling arguments and consideration of the classical structure of the backbone made up of links, nodes, and blobs [6], do not lead to correct estimates of pure advective transport. Between two consecutive nodes, the backbone structure is dominated by its largest blob. Within this blob, transport is influenced by the flow path tortuosity and by the multifractal nature of the velocity field [12]. Moreover, the complexity of the velocity field entails a nontrivial relation between the mean first-passage time of the particles and the mean particle position.

We recall briefly how the mean particle velocity is determined classically by finite-size scaling arguments on a perfect self-similar geometry [8] or on the percolating cluster at threshold [9]. The average time $\langle T\rangle$ spent by a particle in a system of size L is equal to the volume of the system divided by the boundary outflow Q. For the backbone at threshold and for unit potential gradient boundary conditions,

$$\langle T\rangle \sim L^{d_B+\tilde{\mu}-1}, \tag{1}$$

where d_B and $\tilde{\mu}$ are, respectively, the fractal dimension of the backbone and the characteristic exponent of the permeability dependence with scale. Now, $d_B=1.6432\pm0.0008$ and $\tilde{\mu}=0.9826\pm0.0008$ [13], so that $\langle T\rangle \sim L^{1.6258\pm0.0016}$. A consistent numerical result $\langle T\rangle \sim L^{1.64\pm0.02}$ has been found on a dipole geometry [11]. The mean flow velocity $\langle U\rangle$ scales as $L/\langle T\rangle$, i.e., $\langle U\rangle \sim L^{-\psi}$ with $\psi=d_B+\tilde{\mu}-2$.

Based on finite-size scaling arguments [6,8], for spatial scales $\langle R\rangle$ lower than L, the mean velocity should generalize to the form $d\langle R\rangle/dt \sim L^{-\psi} g(\langle R\rangle/L)$, where $\langle R\rangle$ is the average position of the tracer and t is the time. Assuming that velocity is insensitive to L for tracer distances smaller than L, $g(x)\sim x^{-\psi}$ [8], finite-size scaling arguments give by integration,

$$\langle R\rangle \sim t^{1/(1+\psi)}. \tag{2}$$

We derive the time dependence of the mean position of the tracer from the links-blobs structure of the backbone at threshold. At threshold the backbone consists of blobs in series [6] (red links, i.e., singly connected links, are considered as blobs of unit mass). Using the argument of [8] on a blob, the average time spent by a particle in a blob is proportional to the mass of the blob s divided by the flow within the system of size L, that is $s/L^{\tilde{\mu}+1}$. The number of blobs of mass s in a system of size L is $n_s(L)\sim L^{d_r} s^{-(1+d_r/d_B)}$, where d_r is the exponent describing how the number of red links increases with L [14]. The average time spent between two red links separated by R scales as the sum of the times spent in the blobs separating the two red links. As $n_s(L) \sim s^{-1.4564}$ [14], the sum of the times is dominated by the largest time spent in the largest blob. For the same reason, the mass of the backbone between two points separated by R is dominated by the mass of the largest blob, so that the mass of the largest blob scales as R^{d_B} and its size scales as R, a result that we will use below. We thus deduce that the average time spent between two red links separated by R should be

$$\langle t\rangle \sim R^{d_B} L^{\tilde{\mu}-1}, \tag{3}$$

which reduces to Eq. (1) when $R=L$.

In order to analyze the evolution of the spatial and temporal characteristics of the particle plumes, we have set up a numerical experiment on a classical percolating system, made up of unit-length elements whose position and orienta-

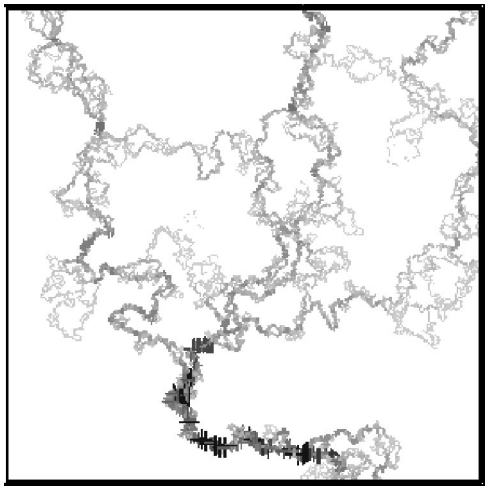

FIG. 1. Flow in the backbone, generated at threshold for which $L=75$ where L is the size of the system. The largest blob lying between the upper edge and the first red link is cut by the system boundary and occupies most of the system. The gray scale is proportional to the flow values with the maximal flow value for the red links represented in black and the minimal values about five orders less than the maximal value represented in light gray.

tion are chosen randomly in a system of size L. The connected cluster is extracted from the system and the flow equation is solved on this structure using Kirchoff's law at the intersections and Darcy's law in the segments (Fig. 1). A detailed description of the used algorithm is given in [15]. The system boundary conditions are a unit potential drop between the two horizontal edges of the system and impervious vertical edges. To simulate transport, we used a standard particle-tracking algorithm, based on flux-weighted distributions of particles at intersections [16]. Particles are introduced along one edge of the system; the probability of a particle entering a segment at this edge is equal to the flow through this segment divided by the total flow through the system. We used 3×10^5 particles for each realization and sampled from 100 to 1000 different realizations for each computation. We checked systematically that the number of particles did not influence the results in a range of 10^3–10^5 particles. Numerical simulations give $\langle T\rangle\sim L^{1.61\pm0.02}$ for L in the range 5–150, which is consistent with the theoretical predictions given by Eq. (1).

The mean $\langle R\rangle$ of the particle positions at a fixed time t and the mean $\langle t\rangle$ of the first-passage time distribution at a fixed position R were computed directly. $\langle R\rangle$ was taken in the time range in which none of the particles leaves the system; this generally occurs when $\langle R\rangle$ reaches about half of L. From intensive numerical simulations for system sizes ranging from $20\leqslant L\leqslant200$ (some of which are shown on Fig. 2), we find that

$$\frac{\langle t\rangle}{\langle T\rangle}\sim\left(\frac{R}{L}\right)^{\tau}\quad\text{with}\quad\tau=0.97\pm0.01, \tag{4}$$

$$\frac{\langle R\rangle}{L}=\left(\frac{t}{\langle T\rangle}\right)^{\rho}\quad\text{with}\quad\rho=0.83\pm0.01, \tag{5}$$

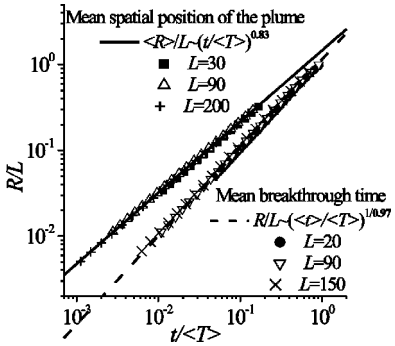

FIG. 2. Normalized mean of the particle positions $(\langle R\rangle(t)/L)$ at normalized fixed time $(t/\langle T\rangle)$ (top points and solid line) and normalized spatial position (R/L) against the normalized average time at which this position is crossed $\langle t\rangle/\langle T\rangle$ (bottom points and dashed line). The solid and dashed lines are the best linear fits to the data.

where $\langle T\rangle$ is given by Eq. (1). Results (4) and (5) differ from the predictions given by finite-scaling arguments (2) and by use of the links-blobs-nodes structure of the backbone (3), respectively. Moreover $\rho\neq1/\tau$, showing that time and spatial averages are not directly related.

We explain first why the estimated and computed mean first-passage times (3) and (4) differ. The average time $d\langle t\rangle$ needed for a particle to cross a slice of width dR depends only on the system geometry. As pointed out by [8], this means, especially, that $d\langle t\rangle$ does not depend on the particular shape of the particle velocity distribution. Rather, $d\langle t\rangle$ scales as the mass of the backbone, i.e., the number of paths $N(R,L)$ times the average path tortuosity $d\langle l\rangle/dR$, divided by the boundary outflow Q [8],

$$\frac{d\langle t\rangle}{dR}\sim\frac{N(R,L)}{Q}\frac{d\langle l\rangle}{dR}. \tag{6}$$

Intensive numerical simulations for R in the range 1–200 and t in the range 10^2–10^6 demonstrate that, independent of t,

$$\langle l\rangle\sim R^{\delta}\quad\text{with}\quad\delta=1.16\pm0.01, \tag{7}$$

$$N(R)\sim R^{\nu}\quad\text{with}\quad\nu=-0.19, \tag{8}$$

leading to $\tau=\delta+\nu$. The decrease of N with R (8) entails a speed up of the particles slightly larger than the slow down due to tortuosity, resulting in a sublinear evolution of the mean first-passage time $\langle t\rangle$ with R.

The decrease of N with R (8) derives from the structure of the backbone. Because the size of the largest blob in a system of size L scales as L, it is likely to be cut by the sides of the system (Fig. 1). In fact our simulations show that the position of the first red link encountered by a particle, defining also the extension of the first blob, is at an average distance of $L/3$ from the system edge. In this truncated blob, the number of paths decreases from the system edge where it is statistically maximal to the first red link where it is equal to one. At scales lower than $L/3$, the geometrical structure relevant to advective transport is a set of tortuous paths of decreasing number N given by Eq. (8), while $\langle t\rangle$ behaves according to Eq. (4). At scales larger than $L/3$, when particles

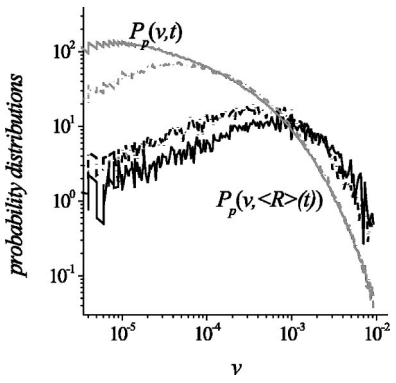

FIG. 3. Comparison of different velocity distributions. Particle velocity distributions at fixed time $P_p(v,t)$ (gray curves) and at the corresponding mean particle position $P_p(v,\langle R\rangle(t))$ (black curves) in a system of size $L=120$. The velocity distribution represented by the solid and dashed lines are taken for $\langle R\rangle(t)$ equal to 5 and 30, respectively.

have statistically crossed the first red link, particles see a series of links and blobs and $\langle t\rangle$ behaves according to Eq. (3). The scaling analysis yields only the first regime.

The estimated and computed mean particle positions (2) and (5) differ also because of the truncation of the largest blob. Finite-size scaling arguments implicitly assume that the largest blob encountered by a particle on a characteristic distance R is smaller than R. In this framework, the anomalous slow advection comes from the increasing probability for the particle to encounter larger blobs and hence smaller velocities. On the contrary, we have seen that the first blob encountered by the particle has a size of the order of the system size. The anomalous transport is thus due to the structure of the first truncated blob rather than to the succession of blobs of varying sizes.

We explain finally why time and spatial averages are not related directly by looking at the particle velocity distribution P_p. The comparison of the particle velocity distributions at fixed times $P_p(v,t)$ (gray curves in Fig. 3) and at the corresponding mean particle positions $P_p(v,\langle R\rangle(t))$ (black curves in Fig. 3) shows that, at fixed times t, particles have smaller velocities than at the corresponding mean positions $\langle R\rangle(t)$. Particles experience a large range of velocities along their path through the system and their probability to be advected by a small velocity increases with time. This tendency is confirmed by the computed mean particle velocities. At evolving times, the mean particle velocity decreases, $\langle v(t)\rangle \sim t^{-0.04}$, whereas for the corresponding mean positions, it increases as $\langle v(\langle R\rangle(t))\rangle \sim t^{0.16}$. These behaviors explain the absence of a simple relation between the temporal and spatial characteristics of the particle plume, $\langle t\rangle(R)$, and $\langle R\rangle(t)$, respectively. It is not only the first moment $\langle v(\langle R\rangle(t))\rangle$ of the velocity distribution $P_p(v,\langle R\rangle(t))$ that changes with $\langle R\rangle(t)$ but more generally the whole distribution $P_p(v,\langle R\rangle(t))$ as shown by the difference of the black solid and dashed line on Fig. 3. The velocity distribution is thus a nonstationary multifractal, with the nonstationarity coming from the spatial variations of the distribution. A unified characterization of the velocity distribution and of its consequences on the spatial and temporal variations of the moments of the particle plume are currently investigated and would be presented in another report.

For systems above the percolation threshold, we verified numerically that, below the correlation length, $\langle R\rangle(t)$ is described by Eq. (5) and not by Eq. (2). Below the correlation length ξ, a particle is likely to be launched into the largest blob and to travel within this largest blob on a tortuous path to reach the first node. Above the correlation length, we found that the advective transport is normal, leading to $\langle R\rangle \sim t$.

To conclude, in the temporal analysis, the mean time of the first-passage time distribution depends only on the system geometry and is conditioned by the largest blob. In the spatial analysis, the mean position of the particles is mostly slowed down by the tortuosity, the velocity being almost constant. When comparing the spatial and temporal approaches, the average time $\langle t\rangle$ to reach the position R is larger than the time to reach the mean position $\langle R\rangle$ [$\langle R\rangle(t)$ lies above $R(\langle t\rangle)$ in Fig. 2] because, for $R(\langle t\rangle)$ all particles have experienced slow velocity zones, increasing their travel time, whereas, for $\langle R\rangle(t)$, particles may still be trapped in the slow velocity zones.

Finally we compare our results to classical transport theories by computing the spatial and temporal standard deviations of particle locations, σ_R and σ_t, respectively. We find that $\sigma_R/\sigma_L \sim (t/\langle T\rangle)^{0.73}$ with $\sigma_L \sim L^{1.1}$ and $\sigma_t/\sigma_T \sim (R/L)^{0.55}$ with $\sigma_T \sim L^{1.39}$. For σ_R, this numerical result differs from $\sigma_R \sim L^{1/(1+\psi)}$, predicted by finite-size scaling arguments [8]. For σ_t, the value of the exponent 0.55 and the above results established on $\langle t\rangle$ show that the first-passage time mean and standard deviation behave almost as for the normal dispersion case, for which $\langle t\rangle \sim R$ and $\sigma_t \sim R^{0.5}$.

The authors thank Harvey Scher and Gennady Margolin for fruitful discussions. This work was supported by the European Commission, Contract No. ENV4-CT97-0456.

[1] J.M. Boggs, S.C. Young, L.M. Beard, L.W. Gelhar, K.R. Rehfeldt, and E.E. Adams, Water Resour. Res. **28**, 3281 (1992).
[2] M.W. Becker and A.M. Shapiro, Water Resour. Res. **36**, 1677 (2000).
[3] G. Dagan, *Flow and Transport in Porous Formations* (Springer Verlag, Berlin, 1989).
[4] B. Berkowitz and H. Scher, Phys. Rev. Lett. **79**, 4038 (1997).
[5] M. Sahimi, *Flow and Transport in Porous Media and Fractured Rock* (VCH, Weinheim, 1995).
[6] D. Stauffer and A. Aharony, *Introduction to Percolation Theory*, 2nd ed. (Taylor and Francis, Bristol, 1992).
[7] S. Havlin and D. Ben-Avraham, Adv. Phys. **36**, 695 (1987).
[8] S. Redner, J. Koplik, and D. Wilkinson, J. Phys. A **20**, 1543 (1987).

[9] M. Sahimi, J. Phys. A **20**, L1293 (1987).
[10] M. Sahimi and A.O. Imdakm, J. Phys. A **21**, 3833 (1988).
[11] Y. Lee *et al.*, Phys. Rev. E **60**, 3425 (1999).
[12] L. de Arcangelis, S. Redner, and A. Coniglio, Phys. Rev. B **34**, 4656 (1986).
[13] P. Grassberger, Physica A **262**, 251 (1999).
[14] H.J. Hermann and H.E. Stanley, Phys. Rev. Lett. **53**, 1121 (1984).
[15] J.R. de Dreuzy, P. Davy, and O. Bour, Water Resour. Res. **37**, 2065 (2001).
[16] B. Berkowitz, C. Naumann, and L. Smith, Water Resour. Res. **30**, 1765 (1994).